



Estimating global chlorophyll changes over the past century



Daniel G. Boyce^{a,b,c,*}, Michael Dowd^d, Marlon R. Lewis^e, Boris Worm^a

^a Department of Biology, Dalhousie University, Halifax, NS B3H 4J1, Canada

^b Department of Biology, Queen's University, Kingston, ON K7L 3N6, Canada

^c Ocean Sciences Division, Bedford Institute of Oceanography, PO Box 1006, Dartmouth, NS B2Y 4A2, Canada

^d Department of Mathematics and Statistics, Dalhousie University, Halifax, NS B3H 4J1, Canada

^e Department of Oceanography, Dalhousie University, Halifax, NS B3H 4R2, Canada

ARTICLE INFO

Article history:

Received 25 July 2013

Received in revised form 28 January 2014

Accepted 29 January 2014

Available online 7 February 2014

ABSTRACT

Marine phytoplankton account for approximately half of the production of organic matter on earth, support virtually all marine ecosystems, constrain fisheries yields, and influence climate and weather. Despite this importance, long-term trajectories of phytoplankton abundance or biomass are difficult to estimate, and the extent of changes is unresolved. Here, we use a new, publicly-available database of historical shipboard oceanographic measurements to estimate long-term changes in chlorophyll concentration (Chl; a widely used proxy for phytoplankton biomass) from 1890 to 2010. This work builds upon an earlier analysis (Boyce et al., 2010) by taking published criticisms into account, and by using recalibrated data, and novel analysis methods. Rates of long-term chlorophyll change were estimated using generalized additive models within a multi-model inference framework, and *post hoc* sensitivity analyses were undertaken to test the robustness of results. Our analysis revealed statistically significant Chl declines over 62% of the global ocean surface area where data were present, and in 8 of 11 large ocean regions. While Chl increases have occurred in many locations, weighted syntheses of local- and regional-scale estimates confirmed that average chlorophyll concentrations have declined across the majority of the global ocean area over the past century. Sensitivity analyses indicate that these changes do not arise from any bias between data types, nor do they depend upon the method of spatial or temporal aggregation, nor the use of a particular statistical model. The wider consequences of this long-term decline of marine phytoplankton are presently unresolved, but will need to be considered in future studies of marine ecosystem structure, geochemical cycling, and fishery yields.

© 2014 Elsevier Ltd. All rights reserved.

1. Introduction

Despite accounting for only 0.2% of global producer biomass, marine phytoplankton account for 46% of annual primary production (Field et al., 1998). Changes in marine phytoplankton biomass or productivity may lead to corresponding changes in geochemical cycles (Redfield, 1958), climate and weather (Murtugudde et al., 2002), fisheries landings (Chassot et al., 2010; Ryther, 1969), and the structure and dynamics of marine ecosystems (Chavez et al., 2003; Richardson and Schoeman, 2004). Although there is mounting evidence that marine phytoplankton concentration is changing at the scale of ocean basins and possibly globally, there is considerable debate regarding the direction and magnitude of change

(Antoine et al., 2005; Behrenfeld et al., 2006; Boyce et al., 2010; Falkowski and Wilson, 1992; Gregg and Conkright, 2002; Gregg et al., 2005; Mackas, 2011; McQuatters-Gollop et al., 2011; Rykaczewski and Dunne, 2011; Venrick et al., 1987). This uncertainty likely results in part from the lack of consistent, long-term time series of estimates of phytoplankton concentration.

Changes in phytoplankton concentration have been inferred from measurements of upper ocean chlorophyll concentration (Chl; mg m^{-3} ; Venrick et al., 1987), transparency (Falkowski and Wilson, 1992), visual estimates of ocean colour (Reid et al., 1998; Wernand and van Der Woerd, 2010), and remotely-sensed water-leaving radiances (Antoine et al., 2005; Behrenfeld et al., 2006; Gregg and Conkright, 2002). Recent trends estimated primarily from satellite data (<30 years) are strongly driven by transient climate fluctuations (Behrenfeld et al., 2006; Boyce et al., 2010; Chavez et al., 2011; Martinez et al., 2009), and longer series are required to resolve long-term trends (Beaulieu et al., 2013; Henson et al., 2010). To overcome this limitation, several studies have combined indices of phytoplankton concentration sampled over

Abbreviations: Chl_T, transparency-derived chlorophyll values; Chl_I, in situ-derived chlorophyll values; Z_D, Secchi depth; FU, Forel-Ule; OGCM, ocean general circulation model; GAM, generalized additive model.

* Corresponding author. Tel.: +1 (902) 448 8941.

E-mail address: Dboyce@dal.ca (D.G. Boyce).

different time periods and from different observational platforms (Antoine et al., 2005; Boyce et al., 2010; Gregg and Conkright, 2002; Gregg et al., 2003; Raitso et al., 2005; Saulquin et al., 2013). One such study combined shipboard measurements of ocean transparency and in situ Chl and concluded that average surface Chl had declined globally over the past century (Boyce et al., 2010). These findings were questioned by others, primarily because of contrasting results from other proxies in some regions (McQuatters-Gollop et al., 2011), and possible calibration issues arising from the merging of two independent time series (Boyce et al., 2011; Mackas, 2011; Rykaczewski and Dunne, 2011). These criticisms were addressed in a follow-up study where time series were calibrated against each other, and their accuracy was compared against more recent satellite-derived measurements of surface Chl (Boyce et al., 2012). This procedure removed any potential bias introduced by merging of data types, and correlated strongly ($r = 0.81$; ranged major axis slope = 1) with the independently derived satellite record. In constructing this database we also introduced a range of methodological advancements and sensitivity analyses, which demonstrated the accuracy of the Chl measurements. Here, we use this larger, and expanded database of Chl measurements (Boyce et al., 2012) combined with newly developed analysis methods and robustness checks to provide new estimates of long-term changes in global upper ocean Chl over the last century.

2. Methods

2.1. Data

Due to the difficulty associated with direct enumeration of phytoplankton and in separating phytoplankton carbon from that contained in other living and detrital particles, the measured concentration of chlorophyll has been widely used as a first-order indicator of the abundance and biomass of oceanic phytoplankton. Despite variability in the phytoplankton Chl-to-carbon ratio (Geider, 1987; Saba et al., 2010), Chl is still the most practical and extensively used proxy of phytoplankton biomass over large spatial scales (Antoine et al., 2005; Behrenfeld et al., 2006; Gregg and Conkright, 2002; Gregg et al., 2005; Henson et al., 2010; Huot et al., 2007; Montes-Hugo et al., 2009; Raitso et al., 2005; Reid et al., 1998).

We use a new and publicly-available database of integrated Chl values collected via shipboard sampling platforms from 1890 to 2010 (details in Boyce et al., 2012). The database is only briefly described here; full details of the data sources, temporal and geographic distribution, quality control and inter-calibration are given in Boyce et al. (2012). It consists of measurements of ocean transparency (derived from Secchi-depth measurements; Z_D) and colour (derived from the Forel-Ule color-matching scale; FU), which were both calibrated against a large and comprehensive database of quality-controlled in situ Chl measurements derived from spectrophotometric or fluorometric analyses of seawater. Since the calibration methods used to derive Chl values are sensitive to the optical properties of the seawater, all near-shore measurements (<20 m water depth or <1 km from the nearest coastline) were removed from the database on the assumption that these waters would likely contain significant concentrations of other optically active constituents, that confound the optical detection of phytoplankton Chl. Statistical techniques were used to identify erroneous measurements; these were corrected or removed from the database.

This database (details in Boyce et al., 2012) has been expanded and improved over a previous version (used by Boyce et al., 2010), in a variety of ways, including:

- (1) The number of individual measurements, and the temporal and spatial coverage of the database has considerably increased, despite the use of more stringent quality control methods.
- (2) Transparency values in the database were calibrated directly against a large number of quality-controlled in situ Chl measurements ($n = 12,841$); this is a large increase over the number of matchups used to calibrate globally distributed remotely sensed water-leaving radiance values from the Coastal Zone Colour Scanner (CZCS; $n = 60$) or the Sea-viewing Wide Field-of-view Sensor (SeaWiFS; $n = 2, 853$; Evans and Gordon, 1994; O'Reilly et al., 2000), and ensures that our calibration equations accurately represent in situ Chl concentrations.
- (3) A range of new statistical methods (*i.e.* spatial filters) were developed to identify potential outlying or implausible Chl measurements in the database, and to subsequently remove or correct them. A range of Chl depth interpolation methods were also explored to verify the assumption that the mean Chl over 20 m was the appropriate metric.
- (4) Measurements in the database were subjected to a number of additional post-calibration analyses testing their quality, precision, and robustness (Boyce et al., 2012). This included testing their accuracy against widely used remote sensing estimates of Chl. These analyses indicated that the Chl values in this database are strongly correlated with Chl from SeaWiFS ($r = 0.81$; ranged major axis slope = 1) on log-log scales. The larger number of matchups and strong correspondence with remote sensing measurements attest to the improved quality of the integrated Chl database (see Boyce et al., 2012 for further details).

Prior to our trend analyses, sensitivity analyses were undertaken to ensure that merging in situ, color, and transparency-derived Chl measurements would not bias the results of subsequent trend analyses. These sensitivity analyses suggested that Chl trends derived from Forel-Ule ocean colour measurements were atypical. Changes in Forel-Ule ocean color determinations are not sensitive to small changes in Chl observed in oligotrophic (blue) waters ($FU < 2$) where the optical properties of pure water dominate, or in mesotrophic (green or brown) waters where other particles and dissolved substances are significant ($FU > 10$). Oligotrophic blue waters contain the lowest Chl concentrations globally and are widely distributed. Because the validity of these values could not be confirmed and to avoid any potential bias, we removed all FU-derived Chl values prior to the trend analysis. The resulting database used here (Table 1) contains 451,383 calibrated Chl values, is globally distributed, and spans over a century (1890–2010). Despite this, the measurements are sparse in many areas, particularly in the Southern hemisphere, and prior to 1950.

2.2. Statistical analyses

Inter-annual changes in average Chl are often small relative to the naturally-occurring variability. For instance, stochastic natural disturbances can drive large transient Chl changes over days to weeks (Hamme et al., 2010), intra-annual Chl variability can span several orders of magnitude in some locations, and inter-annual to decadal climate fluctuations can induce 20-fold changes in Chl over varying time intervals (Barber and Chavez, 1986). Detection of any long-term trends that may underlie this large variability requires powerful and flexible analysis tools. Hence, we estimated changes in Chl over time using generalized additive models (GAMs). GAMs are an extension of widely-used generalized linear models, but enable the estimation of both linear trends as well as non-monotonic responses, (*i.e.* seasonal cycles) within the same

Table 1
Data sources used to estimate Chlorophyll time trends.

Parameter	Symbol	Source	N	Time span	Website
Chlorophyll	Ch _l	WOOD	5315	1900–2003	www.wood.jhuapl.edu/wood/
Chlorophyll	Ch _l	NODC	155,493	1934–2010	www.nodc.noaa.gov/
Chlorophyll	Ch _l	ICES	20,532	1933–2010	www.ices.dk/indexfla.asp
Transparency	Z _D	WOOD	22,266	1903–2008	www.wood.jhuapl.edu/wood/
Transparency	Z _D	NODC	128,988	1899–2007	www.nodc.noaa.gov/
Transparency	Z _D	ICES	17,432	1903–1998	www.ices.dk/indexfla.asp
Transparency	Z _D	MIRC	101,053	1923–1998	www.mirc.jha.jp/en/outline
Transparency	Z _D	BIDA	304	1890–1898	links.baruch.sc.edu/

Table 2
Specification of effects to explain Chl variability (includes linear, discrete, and functional GAM effects according to type of variability explained). The ensemble model set contained different combinations of covariates. The full model contained one effect from each category of variability explained (column 1); the minimum model contained only one effect of inter-annual variability. β are linear and f are functional model effects.

Variability explained	Effect specification	Basis function	Dimension
Inter-annual	$\beta(\text{year})$	NA	NA
	$\beta(\text{factor}(\text{year}))$	NA	NA
	$f(\text{year})$	Cubic	10
Intra-annual	$f(\text{day})$	Cyclic	5
	$f(\text{day} \times \text{factor}(\text{space}))$	Cyclic	5
	$f(\text{day} \times \text{time})$	Tensor product	5,3
	$f(\text{factor}(\text{month}))$	NA	NA
	$f(\text{bathymetry})$	Cubic	4
Nutrient re-suspension	$f(\text{coast distance})$	Cubic	4
Land-based deposition	$f(\text{coast distance} \times \text{factor}(\text{time}))$	Cubic	4
	$f(\text{longitude} \times \text{latitude})$	Thin plate	Estimated
Spatial	$f(\text{longitude})$	Cubic	Estimated
	$f(\text{latitude})$	Cubic	Estimated

model framework (Hastie and Tibshirani, 1986). In contrast to more traditional approaches, GAMs do not require the assumption of a fixed functional form (linear or otherwise), hence more complex (*i.e.* cyclical or bi-modal) dynamics can be captured.

As an additional improvement, we employed GAMs within a multi-model framework (Burnham and Anderson, 2002). This approach uses information theory to rank and/or average across a set of statistical models. By eliminating the reliance on a single model, the robustness of the model inference is improved in much the same way as ensemble forecasts do for meteorological or climate projections. The advantages of this approach are considerable. The GAM approach enables Chl to vary as a linear or non-linear function of our model covariates, while accounting for the non-normality, as well as the spatial and temporal dependence of Chl measurements. The multi-model approach enabled us to allow for a very diverse array of dynamics to explain Chl variability at different ocean locations. For instance, our ensemble models allowed for the strength (magnitude) and nature (linear or smooth) of some important model effects, such as seasonality, or coastal distance to vary across space and through time.

As a first step in the analysis, an ensemble of competing GAM models to explain Chl variability in the upper oceans was selected. The ensemble model set was relatively small (maximum of 20–39 models) and defined a priori according to current knowledge of which factors influence Chl. All ensemble models were estimated from the raw Chl data. Since we were interested in determining the rate of Chl change over time, all ensemble models contained an effect to explain inter-annual Chl variability. In addition to this, most ensemble models included effects to explain variability in Chl related to the location of measurements, the day of the year, water depth, and distance from the shore. Thus the general form of the GAMs used to estimate trends was as follows:

$$\eta(\hat{\mu}_i) = \beta_0 + \beta_{\text{year}} \text{year}_i + \beta_1 x_{1,i} + f_1(x_{2,i}) + f_2(x_{3,i}, x_{4,i}) + \varepsilon_i \quad (1)$$

where i are the individual observations, η is the monotonic link function of the expected mean Chl concentration $\hat{\mu}_i$, year_i , x_1 , x_2 , x_3 ,

and x_4 are predictor variables, β_0 is the model intercept, β denotes parametric and f denotes functional effects estimated from the data, and ε_i represents the residual error term. The functional effects are continuous, smooth curves which can more closely track the response data, and thus accommodate a wide array of response functions ranging from linear to multi-modal (Wood, 2003, 2004, 2006). The predictors (x) in the above example may be spatial (*i.e.* longitude, latitude, bathymetry) or temporal (*i.e.* day of the year, decade) variables explaining Chl variability (Table 2). All ensemble models contained β_{year} , which is a parametric effect capturing the long-term trend in average Chl. For all models we assumed a gamma-distributed error structure ($\hat{\mu}_i \sim \text{Gamma}$) and a log link ($\eta(\hat{\mu}_i) \sim \ln(\hat{\mu}_i)$); alternate distributions and link functions were fitted but did not perform as well. Using this method, we were able to estimate the average rate of Chl change over time while accounting for underlying aspects of Chl variability. Further, because the influence of the model covariates on the mean response is through the logarithmic link function such that $\eta(\beta_{\text{year}}) = e^{\beta_{\text{year}}}$, the estimated rate of Chl change over time was retrieved on a linear response scale ($\text{mg m}^{-3} \text{yr}^{-1}$). All model assumptions, including spatial and temporal dependence were verified by analysis of the model residuals.

All GAMs were fitted to the data using penalized likelihood approximation by penalized iteratively re-weighted least squares (Wood, 2006). The smoothing parameters used to scale the likelihood penalty of all functional effects were estimated by generalized cross-validation. To prevent over-fitting the influence of the effective degrees of freedom on estimation of functional effects was inflated by a factor of 1.4 (Kim and Gu, 2004). The basis dimensions of the functional effects were estimated a priori such that any patterns in the residuals as a function of the functional predictor variables could not be explained by them. More information on the theory and technical aspects of GAMs can be found in, for example Hastie and Tibshirani (1986), Walsh and Kleiber (2001), Wood (2006), Litzow and Ciannelli (2007), while details and examples on their implementation in an oceanographic context may

found in, for example Bigelow et al. (1999), Irwin and Finkel (2009), and Polovina et al. (2008).

The Bayesian information criterion (BIC) was calculated for each individual model within the ensemble (Schwarz, 1978) to evaluate its parsimonious performance. BIC is an information theoretic-based goodness of fit statistic and takes into account model fit, complexity, and sample size,

$$BIC = -2 \ln[L(\theta_p|y)] + p \cdot \ln(n) \quad (2)$$

where n is the sample size, $L(\theta_p|y)$ are the likelihood estimates of the model parameters θ_p , given the data y , and p is the number of free parameters estimated by the model. Normalized multi-model weights for each ensemble model (w_m) were then calculated as,

$$w_m = \frac{\exp\left(-\frac{1}{2\Delta_m}\right)}{\sum_{m=1}^R \exp\left(-\frac{1}{2\Delta_m}\right)} \quad (3)$$

where R represents the total number of models fit, and

$$\Delta_m = BIC_m - BIC_{min}$$

Here BIC_m is the BIC score for model m , and BIC_{min} is the minimum (top ranking) BIC score in the ensemble model set. The 'best' model was selected from the ensemble according to the information-theoretic weights (w_m , Eq. (3)), with $\beta_{year,B}$ extracted as the 'best' model estimated rate of Chl change over time. This approach selects the model containing the largest amount of 'information' (Burnham and Anderson, 2002; Burnham, 2004).

To determine how sensitive the estimated rate of change was to the model selection process, multi-model averaged estimates of Chl change over time were derived as follows,

$$\bar{\beta}_{year,MM} = \sum_{m=1}^R w_m \beta_{year,m} \quad (4)$$

where $\bar{\beta}_{year,MM}$ is the multi-model ensemble-averaged parameter estimate of the rate of Chl change over time, w_m are the model weights, and $\beta_{year,m}$ are the estimates of the rate of Chl change over time for each model.

2.2.1. Estimating trends across spatial scales

We estimated rates of Chl change at local, regional, and global spatial scales, using un-weighted and weighted analysis methods. For the regional analyses Chl change was also estimated as linear, discrete, and smooth functions of time. This was done to evaluate robustness; estimates of change should be relatively insensitive to the use of different statistical methods and assumptions.

To resolve spatial patterns of Chl change, local-scale trends were estimated for individual $10^\circ \times 10^\circ$ cells that contained adequate data. It has been suggested that a continuous Chl series spanning at least 27 (Beaulieu et al., 2013) to as many as 40 years (Henson et al., 2010) is required to separate long-term trends from shorter-term climate-driven fluctuations, with series length varying by ocean region. Hence we restricted our analysis to cells where the temporal range of measurements spanned at least 35 years. We also excluded cells containing <25 individual measurements or <5 individual years with measurements. The remaining database contained $n=280$ individual $10^\circ \times 10^\circ$ cells with sufficient data. For each cell, up to 39 candidate models were fitted to the available data. From this ensemble model set, a multi-model average rate, and a best-model rate of Chl change were estimated (see above, Eqs. (2)–(4)). We calculated the proportion of $10^\circ \times 10^\circ$ cells containing declining or increasing time trends in Chl and estimated 95% confidence intervals about the proportions using the Wilson method (Wilson, 1927). To estimate Chl trends at the 'regional' scale of ocean basins, the data were aggregated into 11 large regions which exhibit similar variability in Chl in response

to seasonality and inter-annual to decadal climate variability (Behrenfeld et al., 2005; Boyce et al., 2010). Although 10 regions were initially selected, observed discontinuities in the Chl response between the eastern ($>20^\circ W$ longitude) and western ($<20^\circ W$ longitude) North Atlantic region led us to further subdivide this basin (see local and regional model results below for further details).

To capture the range of potential Chl trajectories over time, regional trends were estimated from GAMs as linear functions of time (on a log scale) in three different ways: as (1) continuous (linear trend), (2) discrete (decadal average estimates), and (3) smooth functions of time (functional trend). This approach allows both the quantitative (rate) and qualitative (shape) characteristic of trends to be estimated while accounting for the influence of the model covariates.

Rates of Chl change for each region were also determined by aggregating the local $10^\circ \times 10^\circ$ estimates. Individual local scale estimates were heterogeneous in both the uncertainty of individual estimates, as well as the geographic area encompassed by them; statistical weighting methods were used to account for this heterogeneity. For each local estimate, statistical weights were calculated, taking account the sampled area, and the uncertainty weights. Standardized area weights ($w_{area(c,r)}$) were derived for each $10^\circ \times 10^\circ$ cell (c) within each region (r),

$$w_{area(c,r)} = \frac{A_{c,r}}{A_{max(r)}} \quad (5)$$

where $A_{c,r}$ is the convex polygon area of all measurements in cell c within region r and $A_{max(r)}$ is the maximum convex polygon area of all cells within region r . Standardized estimates of uncertainty weights ($w_{uncertainty(c,r)}$) were calculated for each cell (c) within each region (r),

$$w_{uncertainty(c,r)} = \left(\frac{CV_{c,r}}{CV_{max(r)}}\right)^{-1} \quad (6)$$

where $CV_{c,r}$ is the coefficient of variation of cell c within region r , and $CV_{max(r)}$ is the maximum coefficient of variation of all cells within region r . Coefficient of variation values were calculated using the estimated rates of Chl change and standard errors. Using this method, local estimates encompassing larger geographic areas and possessing less uncertainty are allocated greater statistical weight. Weighted mean rates of Chl change for each region ($\bar{\beta}_r$) were estimated as

$$\bar{\beta}_r = \frac{\sum_{c=1}^n w_{c,r} \beta_{c,r}}{\sum_{c=1}^n w_{c,r}} \quad (7)$$

where $w_{c,r}$ are the weights derived as the average of $w_{area(c,r)}$ and $w_{uncertainty(c,r)}$, and $\beta_{c,r}$ are local estimates for change for cell c within region r . Global rates of Chl change were then derived by independently averaging local or regional estimates using the statistical weighting methods (Eqs. (5)–(7)).

Finally, to determine the sensitivity of the estimated trends to the merging of transparency- and in situ-derived Chl measurements (Chl_T and Chl_I, respectively), model II major axis regression models were fitted to matched ($1^\circ \times 1^\circ \times$ month \times year) Chl_T and Chl_I measurements within each $10^\circ \times 10^\circ$ cell (Legendre and Legendre, 1998; Sokal and Rohlf, 1995). The estimated slope parameter from the model (β_{bias}) corresponds to the average change in Chl_T for each unit of Chl_I increase and is estimated as

$$\beta_{bias} = \frac{s_T^2 - s_I^2 + \sqrt{(s_T^2 - s_I^2)^2 + 4(s_{TI})^2}}{2s_{TI}} \quad (8)$$

where s_T^2 and s_I^2 , are the estimated variances of Chl_I and Chl_T, respectively, and s_{TI}^2 is their estimated covariance (Legendre and Legendre, 1998; Sokal and Rohlf, 1995).

3. Results

3.1. Local trends

When considering the 280 $10^\circ \times 10^\circ$ cells with sufficient data for long-term trend analysis, 57.2% (95% Wilson score confidence interval: 51.3–62.8%) showed declining Chl trends; this proportion increased to 60.1% (95% CI: 52.5–67.2%) when only statistically significant trends were considered (Fig. 1A; Table 3). When all 348 available cells were considered irrespective of their trend length, 56.6% showed declining trends. This finding was robust to the estimation of changes using different subsets of the complete Chl database, or when considering all available trends or only statistically significant trends (Table 3). On an area basis, Chl declines were observed over 58.4% of the global ocean surface area where adequate data permitted trend analysis; this proportion increased to 62.1% when considering only areas where the rate of change was statistically significant.

The rate of Chl decline increased with distance from the nearest coastline (Fig. 1B). Weighted linear regression of available local trends ($n = 280$) as a function of distance from the nearest coastline yielded a negative trend, that was marginally non-significant ($-4 \times 10^{-6} \text{ mg m}^{-3} \text{ yr}^{-1} \text{ km}^{-1}$; $P = 0.06$). When considering only statistically significant local-scale estimates of Chl change this relationship became stronger and statistically significant ($-7 \times 10^{-6} \text{ mg m}^{-3} \text{ yr}^{-1} \text{ km}^{-1}$; $P = 0.04$; $n = 168$). This general pattern was also observed when Chl changes were independently

estimated from in situ or transparency derived Chl data, or using only measurements collected since 1950. Estimating local-scale rates of change separately using measurements collected in shelf (<200 m depth) or oceanic (>200 m depth) waters also suggested greater rates of Chl decline in remote open ocean waters (Table 3).

Despite the overall decline in Chl observed, statistically significant increases were observed in 39.9% of cells and (or 38.0% of the ocean surface) where adequate data permitted trend analysis. Clusters of increasing cells were observed in the temperate North Pacific, in the Northeast Atlantic, and across the subtropical warm pool (Fig. 1A). Although rates of Chl increase were greater in waters closer to the shorelines (Fig. 1B), there was no change in the proportion of cells containing increasing Chl trends in coastal (<200 m depth; 59.6%) or oceanic (>200 m depth; 60.3%) waters.

Estimated rates of Chl change were larger and more variable in the Southern Hemisphere, likely as a function of limited data availability. Spatial examination of the strength of inference for the main model effects suggested the seasonal effects were of large importance in most cells, but were especially significant in the Northern Hemisphere and in the Atlantic Ocean. Spatial effects were dominant in the tropical Pacific Ocean (20°N to 20°S), where seasonal effects were weaker.

When all local estimates were aggregated by ocean region ($n = 11$; Fig. 1C) using statistical weighting methods (Eqs. (5)–(7)), declining trends were observed in 8 of 11 regions; five of those were statistically significant (Fig. 1D). The largest rates of decline were observed in the Atlantic, the South Indian, and the Southern Ocean

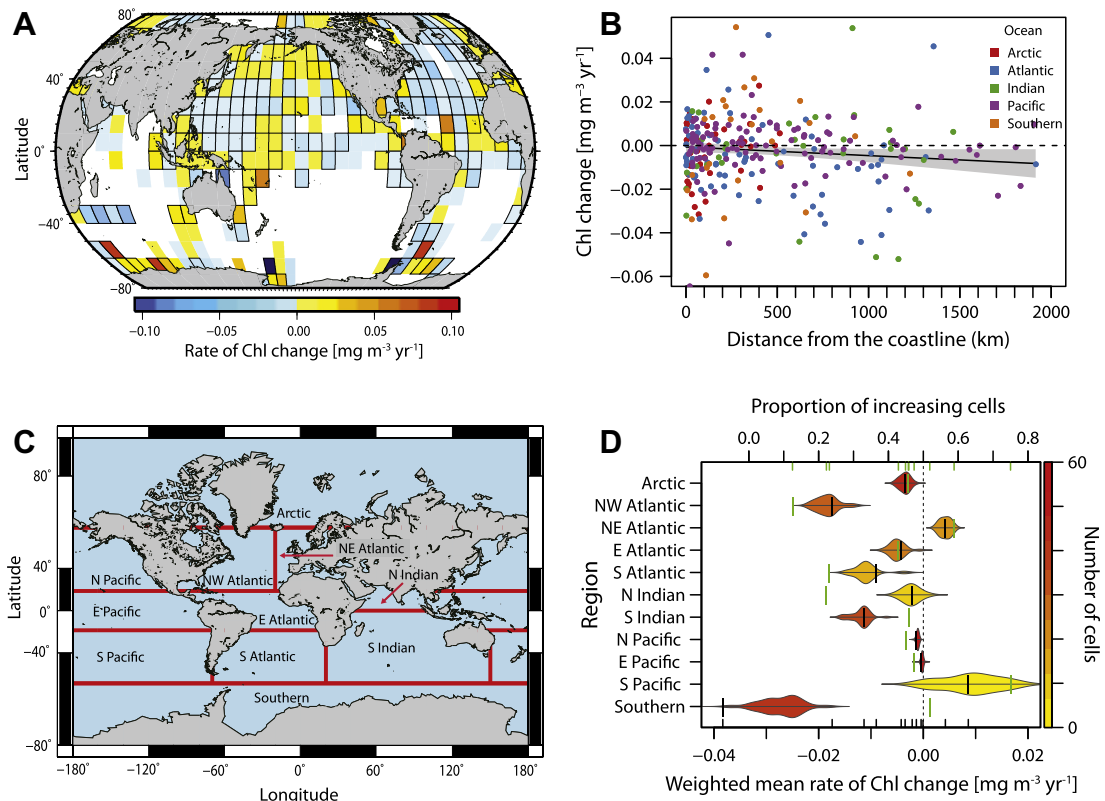


Fig. 1. Local-scale phytoplankton trends. (A) Estimated instantaneous linear rate of Chl change in each $10^\circ \times 10^\circ$ cell ($n = 280$). Color coding indicates the average rate of change over the available time series. Cells bordered in black denote statistically significant rates of change ($P < 0.05$) and white cells indicate cells with insufficient data. (B) Chl change in each $10^\circ \times 10^\circ$ cell as a function of distance from the nearest coastline (km). Colours indicate the ocean where the cell was located. Solid trend line was derived from a weighted linear model; shaded area is the 95% confidence interval; dashed line represents no change in Chl. (C) Ocean regions ($n = 11$) used to estimate regional trends in Chl. (D) Weighted mean Chl changes estimated by aggregating local estimates within each region. Shapes ('Raindrops') represent the probability distribution of the individual local estimates. The weighted mean rates of Chl change are depicted as black vertical lines, and the width of the raindrops and gray horizontal lines are the 95% confidence limits about the means. The colours of the raindrops depict the number of cells within each region. Green vertical lines are the proportion of increasing cells within each region. Black and green tick marks on the axes represent the individual rates or proportions of change, respectively. Dashed line represents no change.

Table 3
 Summary statistics from local-scale estimates of Chl change estimated from different data sets. N cells are the number of 10° × 10° cells, % declining is the proportion of all cells that contain declining trends, weighted mean rate are the average weighted rates of Chl change (mg m⁻³ yr⁻¹), Mean rate is the arithmetic mean rate of Chl change, 95% CI are the confidence intervals for the weighted and average rates of change, N/cell is the median number of measurements per cell, year span is the years spanned by all data.

Measurements Used	N cells	% Cells declining	Weighted mean rate	±95% CI	Mean rate	±95% CI	N/cell	Year span
<i>All trends</i>								
ALL	280	0.57	-0.0023	0.001	-0.0039	0.042	321	1890–2010
1950 Onward	254	0.55	-0.0026	0.002	-0.0040	0.046	311	1951–2010
Truncated	252	0.58	-0.0016	0.001	-0.0029	0.032	336	1890–2010
Chl _r	153	0.51	0.0002	0.001	0.0004	0.030	329	1890–2008
Chl _l	147	0.48	-0.0036	0.003	-0.0051	0.069	194	1900–2010
Shelf (<200 m depth)	72	0.58	0.0000	0.002	-0.0038	0.030	474	1891–2010
Oceanic (>200 m depth)	208	0.57	-0.0031	0.001	-0.0040	0.046	268	1890–2010
<i>Significant trends</i>								
ALL	168	0.6	-0.0032	0.001	-0.0063	0.053	478	1890–2010
1950 Onward	152	0.57	-0.0038	0.002	-0.0069	0.058	433	1951–2010
Truncated	137	0.63	-0.0026	0.001	-0.0042	0.039	527	1890–2010
Chl _r	91	0.51	0.0005	0.002	0.0015	0.037	445	1890–2008
Chl _l	92	0.55	-0.0061	0.004	-0.0095	0.085	291	1900–2010
Shelf (<200 m depth)	47	0.6	0.0000	0.003	-0.0052	0.036	809	1891–2010
Oceanic (>200 m depth)	121	0.6	-0.0046	0.002	-0.0067	0.058	434	1890–2010

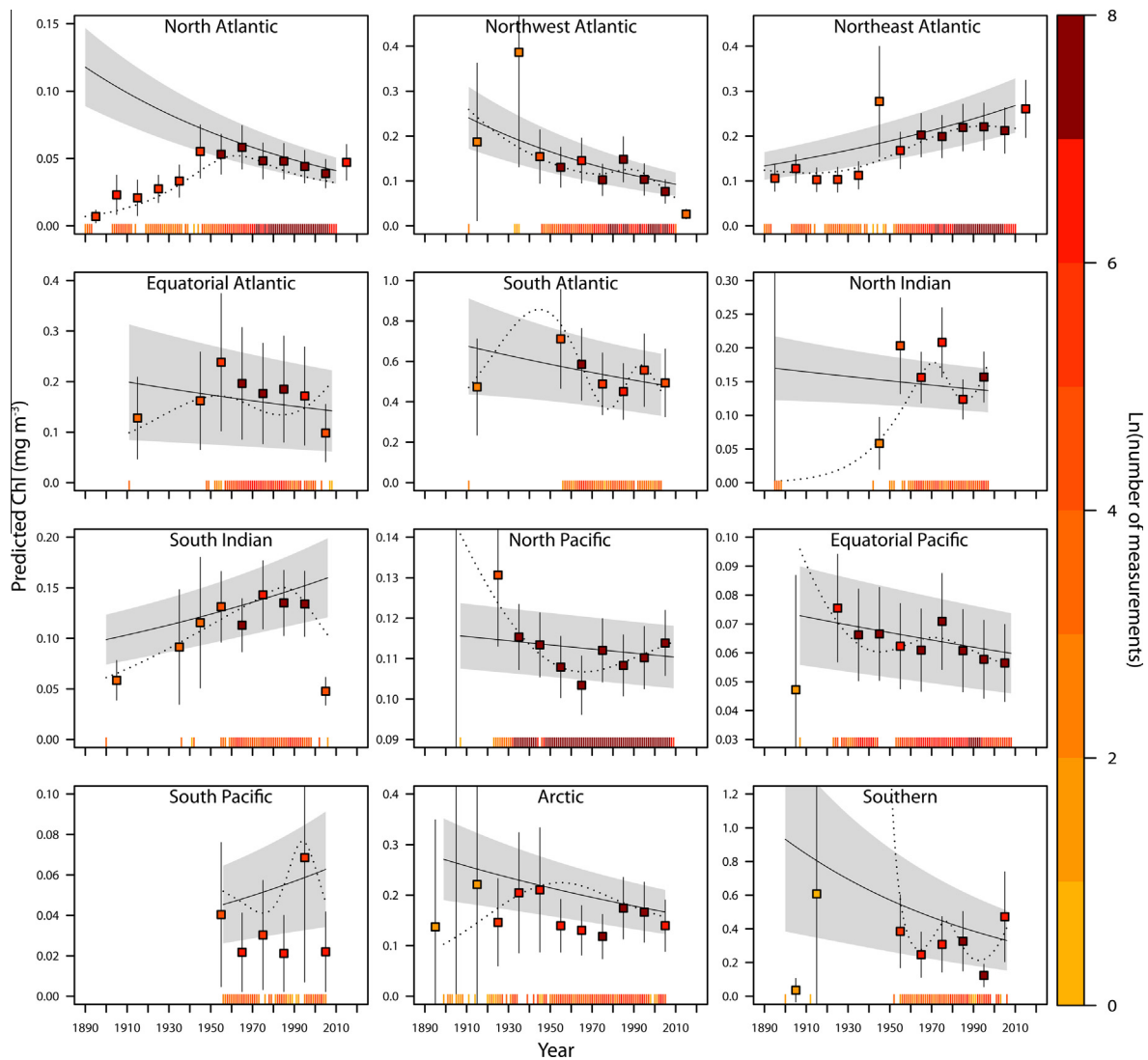


Fig. 2. Temporal trajectories of phytoplankton. Estimates of relative Chl as a discrete (square points), log-linear (lines), and smooth (dotted lines) function of temporal variability in each region ($n = 11$). Tick marks on the x-axis represent the availability of data through time. The color of tick marks and points represents the scaled number of observations available in each year (tick) and decade (point). Shaded areas represent approximate 95% Bayesian credible limits around each log-linear trend. The magnitudes of predicted Chl are not exact, but rather representations which depend on the values of the model covariates selected for prediction.

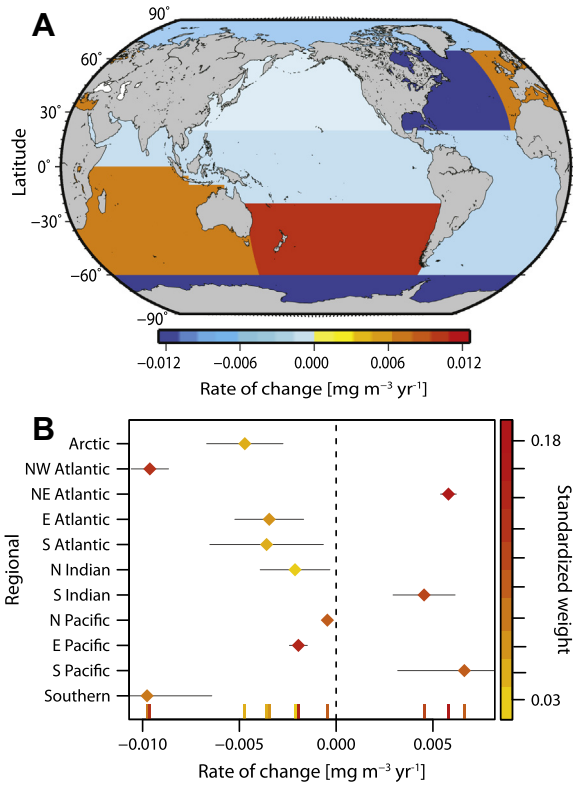


Fig. 3. Regional-scale phytoplankton trends. (A) Estimated instantaneous linear rate of Chl change in each of 11 ocean regions. Colors indicate rate of change; yellow and red are increasing regions, blue are declining regions. (B) Chl changes estimated for each region (points), with 95% confidence intervals (gray lines). Individual estimates are displayed as tick marks on the x-axis. Colors depict the standardized statistical weight used in the derivation of the global average for each region. Dashed line represents no change.

region. Conversely, the Northeast Atlantic and South Pacific showed increasing trends and the equatorial Pacific region appeared approximately stable. Estimates of change in the Southern hemisphere regions were found to be more variable and uncertain than elsewhere. The proportion of declining cells was also greater than 50% in 9 of 11 regions, with the largest proportional declines in Atlantic and North Indian regions (Fig. 1D). The proportional changes of cells within each region was similar to weighted averages rates, except for the Southern Pacific and Southern regions, where the number of cells and measurements were small and estimates of change were variable (Fig. 1D).

Table 4

Regional-scale estimates of Chl change. Estimate, SE, and *P*-value are the instantaneous linear rate of Chl change (mg m⁻³ yr⁻¹), standard errors, and *P* values for the rates of change. % per Year and % are the Chl change per year and total % change, reported as a proportion of the initial value, Deviance is the proportion of deviance explained by the individual models, Area is the maximum polygon area encompassed by the available data (km² × 10⁴) and N/Year is the average number of measurements available in each year.

Region	Estimate	SE	<i>P</i> -value	% yr ⁻¹	%	Deviance	Area	Year span	N/yr ⁻¹
Arctic	-0.0047	0.001	<0.0001	-0.37	-39.2	35	177	1899–2005	111
NW Atlantic	-0.0096	0.0005	<0.0001	-0.62	-61.4	48	295	1911–2010	781
NE Atlantic	0.0058	0.0002	<0.0001	0.84	100.8	45	183	1890–2010	730
E Atlantic	-0.0035	0.0009	0.0001	-0.29	-28.1	65	384	1911–2008	190
S Atlantic	-0.0036	0.0015	0.0164	-0.31	-28.5	43	299	1911–2003	60
N Indian	-0.0021	0.0009	0.0208	-0.19	-19.4	59	196	1895–1997	84
S Indian	0.0045	0.0008	<0.0001	0.58	61.5	76	760	1900–2006	131
N Pacific	-0.0005	0.0001	<0.0001	-0.04	-4.1	52	478	1907–2009	2842
E Pacific	-0.002	0.0002	<0.0001	-0.18	-18.2	78	964	1907–2008	475
S Pacific	0.0066	0.0018	0.0002	0.78	38.2	69	565	1956–2005	53
Southern	-0.0098	0.0017	<0.0001	-0.61	-64.7	40	336	1900–2006	89

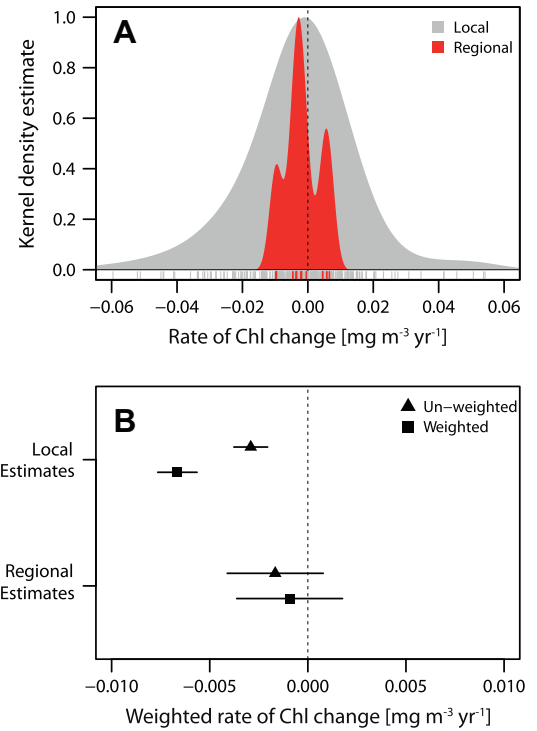


Fig. 4. Average global phytoplankton change. (A) Shaded areas represent the standardized kernel density distribution of individual local (gray) and regional (red) scale estimates of Chl change. Tick marks on the x-axis are the values of the individual estimates of change. Dashed line represents no change. (B) Globally averaged rates of Chl change estimated using local and regional scale estimates. Global rates of change were calculated as un-weighted (triangle points) and weighted (square points); random-effects were assumed. Horizontal lines are the 95% confidence limits around the mean rates; dashed line represents no change. (For interpretation of the references to colour in this figure legend, the reader is referred to the web version of this article.)

3.2. Regional trends

Chl trajectories estimated as discrete, linear, or smooth functions of time suggested strong fluctuations in average Chl concentrations superimposed on long-term linear trends (Fig. 2), with most trajectories declining over the last 60 years. Again, estimated Chl trends were more uncertain in the Southern Hemisphere regions and over earlier time periods, likely as a function of limited data availability. Estimated smooth Chl trajectories are strongly influenced by data-poor years and decades, possibly explaining the large fluctuations over the pre-1950 period (Fig. 2). With the exception of the Pacific regions, Chl was observed to initially

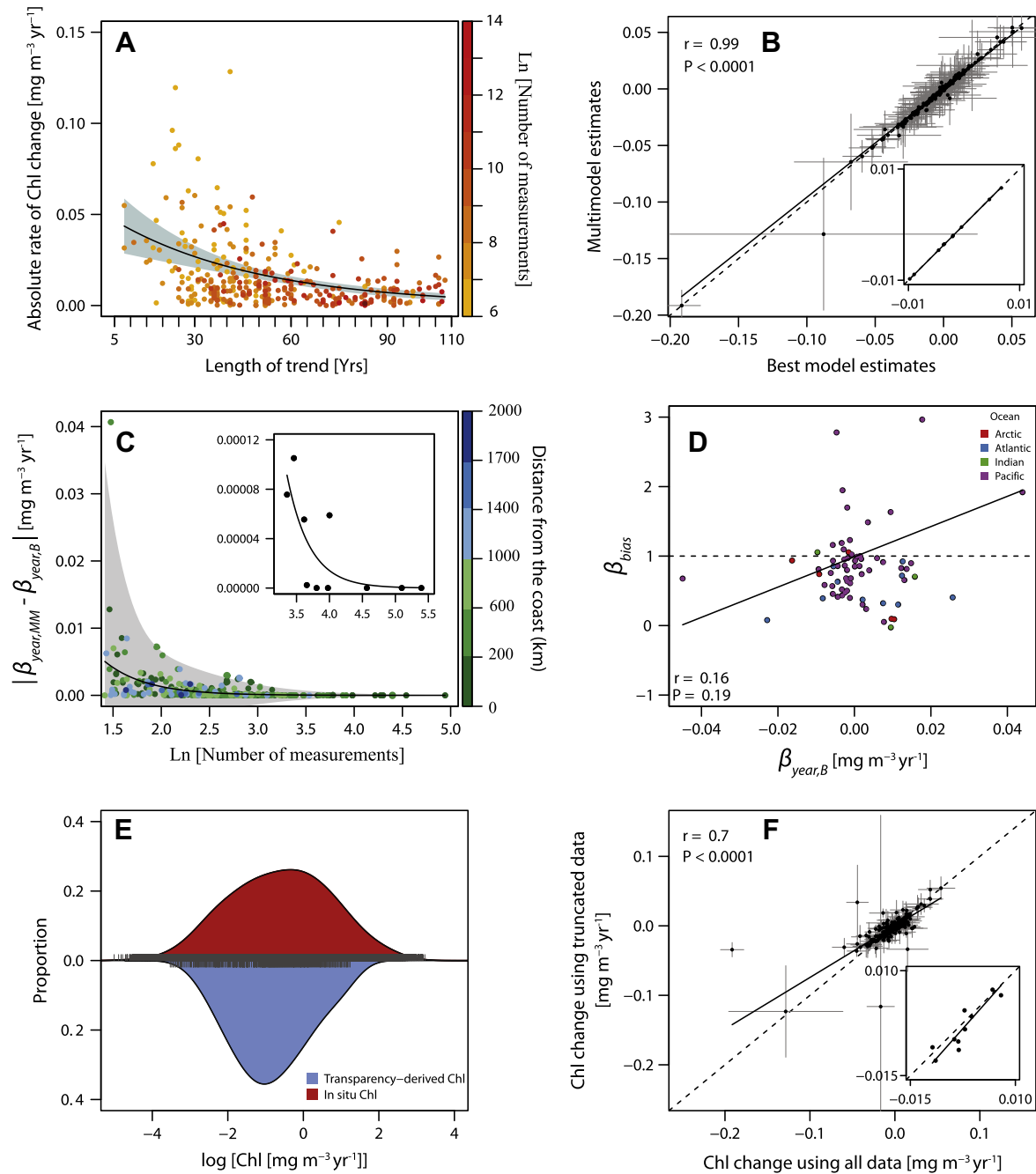


Fig. 5. Sensitivity and robustness analyses. (A) The absolute estimated rate of Chl change for each $10^\circ \times 10^\circ$ cell is plotted as a function of trend length. Colors represent the number of measurements in each cell. The relationship was best approximated by a generalized linear model ($\hat{\mu}_i \sim \text{Gamma}$ and $\eta(\hat{\mu}_i) \sim \ln(\hat{\mu}_i)$; solid line); Shaded area depicts the confidence limits. (B) Rates of Chl change estimated by multi-model averaging plotted against best-model estimates for each $10^\circ \times 10^\circ$ cell. Gray lines are the 95% confidence intervals for the estimates; dashed line represents idealized relationship (slope = 1, intercept = 0). Solid line is the model II regression fit ($r = 0.99$; $P < 0.0001$). Inset displays the same relationship for regional estimates. (C) Difference between multi-model averaged and best model rates of Chl change as a function of log sample size for each $10^\circ \times 10^\circ$ cell. The relationship was approximated by a generalized linear model ($\hat{\mu}_i \sim \text{Poisson}$ and $\eta(\hat{\mu}_i) \sim \ln(\hat{\mu}_i)$; solid line); shaded area depicts the 95% confidence interval. Colours represent the distance of the cell to the nearest coastline. Inset displays the same relationship for regional estimates. (D) Estimated rates of change from all data plotted as a function of the average difference (model II major axis linear regression slope; Eq. (8)) between Chl data types for each $10^\circ \times 10^\circ$ cell. Fitted line represents the relationship estimated from a model II linear regression. Colour depicts the ocean where trends were estimated. (E) Probability distribution of log-transformed Chl_I (red) and Chl_T (blue) measurements estimated as a kernel density function. Area under each curve sums to 1. Tick marks represent the exact Chl values. (F) Rates of Chl change estimated using truncated data as a function of changes estimated from all available data for each $10^\circ \times 10^\circ$ cell. Gray lines are the 95% confidence intervals for the estimates; solid line represents slope from a model II regression fitted to the data ($r = 0.7$; $p < 0.0001$). Dashed line represents idealized relationship (slope = 1, intercept = 0). Inset is the same relationship for regional estimates.

increase before undergoing prolonged decline. Most of these initial increases predated 1950, and appeared to be driven by a relatively small number of data points.

Estimates of change within large ocean regions described previously (Fig. 1C), indicated statistically significant Chl decline in 8 of 11 regions (Fig. 3A and B; Table 4). The largest instantaneous rates

of decline were observed in the Southern Ocean ($-0.0098 \pm 0.0033 \text{ mg m}^{-3} \text{ yr}^{-1}$; $P < 0.001$), Northwest ($-0.0096 \pm 0.001 \text{ mg m}^{-3} \text{ yr}^{-1}$; $P < 0.001$), Arctic ($-0.0046 \pm 0.002 \text{ mg m}^{-3} \text{ yr}^{-1}$; $P < 0.001$), South ($-0.0036 \pm 0.0029 \text{ mg m}^{-3} \text{ yr}^{-1}$; $P < 0.001$), and equatorial ($-0.0035 \pm 0.0018 \text{ mg m}^{-3} \text{ yr}^{-1}$; $P < 0.001$) Atlantic and regions (instantaneous rate of change and 95% confidence interval).

Statistically significant rates of increase were observed in the Northeast Atlantic ($0.0045 \pm 0.0016 \text{ mg m}^{-3} \text{ yr}^{-1}$; $P < 0.001$), South Indian ($0.0058 \pm 0.0004 \text{ mg m}^{-3} \text{ yr}^{-1}$; $P < 0.001$), and South Pacific ($0.0066 \pm 0.0005 \text{ mg m}^{-3} \text{ yr}^{-1}$; $P < 0.001$) regions. When extrapolating over the available trend length, these rates correspond to substantial cumulative upper ocean Chl changes. When calculated from the annual proportional changes (Table 4), the largest cumulative proportional declines were observed in the Northwest Atlantic (−61.4%), Southern (−64.7%), and Arctic (−39.2%) regions (Table 4). Smaller declines were calculated for the equatorial Atlantic (−28.1%) and South Atlantic (−28.5%), North Indian (−19.4%), North (−4.1%) and equatorial Pacific (−18.2%) regions. Large increases were extrapolated for the Northeast Atlantic (+100.8%), South Indian (61.5%) and South Pacific (38.2%) regions. These rates of change may be exaggerated for regions where data availability is low such as the Southern Ocean. In such instances, rates of change could be inflated due to the influence of measurements taken in more recent, data-rich decades.

3.3. Global trends

When aggregated globally, both local and regional scale estimates of change were approximately Gaussian distributed (Fig. 4A). Using statistical weighting methods to account for differences in the uncertainty and spatial coverage of estimates, we observed globally declining Chl trajectories. Synthesis of local estimates revealed, in aggregate, a statistically significant global Chl decline of $-0.0066 \pm 0.001 \text{ mg m}^{-3} \text{ yr}^{-1}$ (random-effects weighted mean and 95% confidence interval). This finding was insensitive to the use, or method, of weighting (Fig. 4B). Synthesis of available regional estimates suggested that the global rate of change was smaller and not statistically significant ($-0.0009 \pm 0.0027 \text{ mg m}^{-3} \text{ yr}^{-1}$). The global rate of change derived from regional estimates was sensitive to the splitting of the North Atlantic region; when analyzing the North Atlantic as a whole, the global rate was greater and statistically significant ($-0.0029 \pm 0.0025 \text{ mg m}^{-3} \text{ yr}^{-1}$).

3.4. Sensitivity and robustness analyses

Analyses of all available $10^\circ \times 10^\circ$ cells suggested that as the length of the available Chl time series decreases, the estimates of change become larger and more uncertain (Fig. 5A). This supports the contention that Chl trends estimated over shorter timescales are strongly influenced by decadal-scale climate oscillations and may not necessarily represent long-term trends (Henson et al., 2010; Martinez et al., 2009). However, since sample size also covaries with trend length, it is possible that the larger magnitude and uncertainty of estimates may be driven by data density, not just total time span. The estimated rates and patterns of Chl change at local scales were broadly insensitive to model specification, or the spatial resolution chosen (changes within $5^\circ \times 5^\circ$ cells were also estimated). The proportion of declining cells and average global rate of Chl change were largely unchanged.

To determine the sensitivity of our analysis to model averaging, the estimates of Chl change over time from best models ($\beta_{\text{year},B}$) were compared against those derived from multi-model averaging ($\bar{\beta}_{\text{year},MM}$; Fig. 5B). In almost all instances, $\bar{\beta}_{\text{year},MM}$ and $\beta_{\text{year},B}$ were identical in direction, but differed slightly in magnitude. The $\bar{\beta}_{\text{year},MM}$ estimates were generally smaller than $\beta_{\text{year},B}$ estimates and the differences between them tended to increase with decreasing sample size (Fig. 5C). However, since differences between $\bar{\beta}_{\text{year},MM}$ and $\beta_{\text{year},B}$ were small and because the statistical theory underlying single model selection is more robust, $\beta_{\text{year},B}$ was used as the metric of Chl change. The overall results were insensitive to the use of $\bar{\beta}_{\text{year},MM}$ or $\beta_{\text{year},B}$.

Several analyses were performed to determine the sensitivity of the estimated trends to the blending of Chl measurements collected from different sampling platforms. It has been suggested that since the transparency- and in situ-derived Chl values are available over different time periods, any systematic difference between them could bias the overall rate of change over time (Mackas, 2011; Rykaczewski and Dunne, 2011). We conducted several analyses to explore this possible bias. Firstly, if temporal sampling differences were biasing the Chl trends, the magnitude of the bias should scale proportionally to the magnitude of the trends. To quantitatively test this, we examined the linear scaling of space- and time-matched Chl_T and Chl_I values on log–log scales in conjunction with the trend estimated from the integrated data ($\beta_{\text{year},B}$) for each individual $10^\circ \times 10^\circ$ cell. The linear scaling parameter was estimated as the model II major axis log–log regression slope of Chl_T against Chl_I (β_{bias}), whereby parameter values greater than 1 indicate $\text{Chl}_T > \text{Chl}_I$ (Eq. (8)). If declining Chl trends were the result of a bias resulting from the blending of different data sources, β_{bias} should be negatively related to $\beta_{\text{year},B}$. There was no indication that a systematic bias was present ($r^2 = 0.01$, $P = 0.19$), suggesting that the estimated Chl trends ($\beta_{\text{year},B}$) are not an artifact of the blending of Chl_T and Chl_I (Fig. 5D).

Whereas the Chl_I measurements in the integrated database contain intrinsic measurement error, the Chl_T values are calibrated using a deterministic process and thus contain only an indirect form of measurement error. Consequently the means of Chl_T and Chl_I are identical, but their variances may not be (Fig. 5E). Analyses were performed to determine the possible effect of this uneven variance on the estimated Chl trends. Trends were estimated using only Chl measurements that were within the extreme tails of the Chl_T distribution. This truncation simulation effectively standardized the variances of Chl_I and Chl_T . By comparing trends estimated from the truncated data against those estimated using all data, the sensitivity of the trends to the potentially uneven variances of Chl_T and Chl_I may be assessed. This analysis suggested that the trends were insensitive to the larger variance of Chl_I measurements (Fig. 5F). The changes estimated from the truncated database indicated a slightly greater proportion of declining 10° cells and greater rates of Chl decline.

4. Discussion and conclusion

This analysis presents comprehensive empirical evidence for a decline in average Chl across the majority of the global ocean, particularly over the second half of the 20th century. Importantly, this work builds upon previous estimates of long-term phytoplankton change (Boyce et al., 2010) and addresses all critical comments which were published in response (Boyce et al., 2011; Mackas, 2011; McQuatters-Gollop et al., 2011; Rykaczewski and Dunne, 2011). We have increased the robustness of this analysis in several ways including:

- (1) Using a larger Chl database with more stringent data quality control methods and direct Chl calibration methods (full details in: Boyce et al., 2012).
- (2) Implementing a range of new analyses to ascertain the sensitivity of the estimated trends to any possible biases (Mackas, 2011; Rykaczewski and Dunne, 2011).
- (3) Using multi-model analyses to eliminate the reliance on a single model of Chl change, and enabling for more complex Chl dynamics to be tested.
- (4) Restricting our analysis to Chl time-series that span at least 35 years, to minimize any confounding with cyclical climate variability (Beaulieu et al., 2013; Henson et al., 2010).

Following these improvements, the trajectories of Chl change reported here are similar, but not identical, to those estimated previously (Boyce et al., 2010). Statistically significant chlorophyll declines were observed in $60.1 \pm 0.076\%$ of 10° cells examined, and over 62% of the global ocean surface area where trend analysis was possible. While Chl has declined over most of the ocean, Chl trends were spatially heterogeneous. Large clusters of declining cells were observed across the mid- to high-latitude Atlantic oceans, the western Pacific and the eastern tropical Pacific Oceans (Fig. 1A). Patches of increasing cells were found in the North Pacific Ocean, northeast Atlantic Ocean, and Mediterranean Sea (Fig. 1A). The greatest rates of Chl change were observed in the Southern Hemisphere ($<50^\circ\text{S}$), and where the trend time span was shorter, likely as a function of limited data availability.

Weighted linear regression analysis suggested that the rate of Chl change became increasingly negative with increasing distance from land masses, ($p < 0.01$). This suggests that Chl in the open oceans has been declining more rapidly than in shelf areas. This finding is in agreement with results derived from satellite data over more recent time periods (1997 to ~ 2007), documenting declining phytoplankton in the open oceans (Gregg et al., 2005; Vantrepotte and Melin, 2009; Ware and Thomson, 2005) and expansion of the oligotrophic gyres (Polovina and Woodworth, 2012; Polovina et al., 2008). These declining trends have been generally related to ocean warming, intensifying vertical stratification and reduced vertical mixing (Behrenfeld et al., 2006; Boyce et al., 2010; McClain and Signorini, 2004; Polovina et al., 2008), although they are largely unexplored over pre-satellite eras. Stable or increasing trends in shelf areas, could be, at least in part, due to the effects of anthropogenic eutrophication (Jickells, 1998; Nixon, 1995; Peierls et al., 1991), which may counteract the effects of increasing stratification on nutrient supply rates.

Regional estimates of change were in general agreement with local estimates, with the largest declines observed in the Atlantic (excluding the Northeast Atlantic), and polar regions (Figs. 2 and 3). Due to the large spatial scale of these estimates, and because the minimum trend length of our analysis is 35 years, it is challenging to compare our results to independently published estimates, almost all of which are estimated at finer spatial scales (Reid, 1975; Reid et al., 1998; Saba et al., 2010; Venrick et al., 1987), or over shorter time intervals (Antoine et al., 2005; Behrenfeld et al., 2006; Goes et al., 2005; Gregg et al., 2005; Montes-Hugo et al., 2009). Despite this, some general patterns appear to emerge.

Local and regional declines in the North Pacific were broadly supported by independent long-term estimates derived from ocean transparency (Falkowski and Wilson, 1992) or colour (Wernand and van Der Woerd, 2010). Our estimated rate of decline for the North Pacific region ($-0.0005 \text{ mg m}^{-3} \text{ yr}^{-1}$) is similar but smaller than that estimated over a shorter time interval ($-0.002 \text{ mg m}^{-3} \text{ yr}^{-1}$; 1900–1981) by Falkowski and Wilson (1992).

Long-term local and regional Chl changes in the North Atlantic are in agreement as well with estimated changes in the phytoplankton colour index (PCI) from the North Sea and Northeast Atlantic using the continuous plankton recorder (CPR) survey (Raitso et al., 2005; Reid, 1975; Reid et al., 1998), but at odds with PCI estimates from the Central Northeast Atlantic (52° to 58°N and 10° to 20°E). Changes in Chl across the Northeast Atlantic since ~ 1978 estimated from remote sensing measurements are spatially variable, but when averaged spatially also agree with our estimates, and are suggestive of a declining trend (Antoine et al., 2005; Gregg and Conkright, 2002). Indeed, both our analysis and those using the phytoplankton color index or remote sensing data suggest that phytoplankton changes across the North Atlantic are spatially heterogeneous (Antoine et al., 2005; Behrenfeld et al., 2006; Gregg and Conkright, 2002; Reid, 1975; Reid et al., 1998).

This heterogeneity also extends to time trends, and Chl time trends based on empirical estimates (Antoine et al., 2005; Boyce et al., 2010; Gregg and Conkright, 2002; Reid, 1975; Reid et al., 1998) and future predictions (i.e. Henson et al., 2010; Olonscheck et al., 2013; Steinacher et al., 2010) are notably variable. Our analysis suggests that different dynamics may explain phytoplankton variability in the eastern and western portions of the North Atlantic region (Fig. 2), and that estimating a single aggregate trend for the entire region may be inappropriate.

Globally, the direction of long term secular trends described here is consistent with ocean general-circulation model (OGCM) projections of future changes in Chl over similar time horizons. Although there is substantial variability among OGCM projections, 15 of 18 published estimates report declining marine Chl or primary production into the future (median time interval: 100 yr; time interval range: 10–2000 yr; Beaulieu et al., 2013; Bopp et al., 2001; Boyd and Doney, 2002; Cermenio et al., 2008; Cox et al., 2000; Henson et al., 2010; Hofmann et al., 2011; Olonscheck et al., 2013; Steinacher et al., 2010; Taucher and Oschlies, 2011). These models do not account for biological interactions, which may modify the Chl time trends (O'Connor et al., 2009; Olonscheck et al., 2013; Taucher and Oschlies, 2011).

We conclude that average upper ocean chlorophyll concentrations have declined over the past century but that the absolute magnitude of this change remains uncertain (global averages from local and regional models were both negative, but varied by a factor of 7). The rates of change we report are also heterogeneous in space and time and are overlaid by multi-decadal variability. Our analysis suggests that the direction of upper ocean Chl change is robust (i.e. consistently declining, on average), but the magnitude of changes is sensitive to the scale at which data are aggregated. A major source of this uncertainty stems from the limited availability of Chl measurements in many regions and years. This uncertainty and the fundamental importance of marine phytoplankton should provide a powerful incentive to increase global observational capabilities in order to more accurately resolve long-term phytoplankton change.

Acknowledgements

We are very grateful to all data providers, to J. Mills-Flemming for statistical advice. Funding was provided by the Natural Sciences and Engineering Research Council of Canada.

References

- Antoine, D., Morel, A., Gordon, H.R., Banzon, V.F., Evans, R.H., 2005. Bridging ocean color observations of the 1980s and 2000s in search of long-term trends. *Journal of Geophysical Research* 110, 1–22.
- Barber, R.T., Chavez, F.R., 1986. Ocean variability in relation to living resources during the 1982–83 El Niño. *Nature* 319, 279–285.
- Beaulieu, C., Henson, S.a., Sarmiento, J.L., Dunne, J.P., Doney, S.C., Rykaczewski, R.R., Bopp, L., 2013. Factors challenging our ability to detect long-term trends in ocean chlorophyll. *Biogeosciences* 10, 2711–2724.
- Behrenfeld, M.J., Boss, E., Siegel, D.A., Shea, D.M., 2005. Carbon-based ocean productivity and phytoplankton physiology from space. *Global Biogeochemical Cycles* 19, 1–14.
- Behrenfeld, M., O'Malley, R., Siegel, D., McClain, C., Sarmiento, J., Feldman, G., Milligan, A., Falkowski, P., Letelier, R., Boss, E., 2006. Climate-driven trends in contemporary ocean productivity. *Nature* 444, 752–755.
- Bigelow, K.A., Boggs, H., He, X.L., 1999. Environmental effects on swordfish and blue shark catch rates in the US North Pacific longline fishery. *Fisheries Oceanography*, 178–198.
- Bopp, L., Monfray, P., Aumont, O., Dufresne, J.-L.L., Le Treut, H., Madec, G., Terray, L., Orr, J.C., 2001. Potential impact of climate change on marine export production. *Global Biogeochemical Cycles* 15, 81–99.
- Boyce, D., Lewis, M., Worm, B., 2010. Global phytoplankton decline over the past century. *Nature* 466, 591–596.
- Boyce, D., Lewis, M.R., Worm, B., 2011. Boyce et al. reply. *Nature* 472, E8–E9.
- Boyce, D.G., Lewis, M., Worm, B., 2012. Integrating global chlorophyll data from 1890 to 2010. *Limnology and Oceanography: Methods*, 10, 840–852.

- Boyd, P.W., Doney, S.C., 2002. Modelling regional responses by marine pelagic ecosystems to global climate change. *Geophysical Research Letters* 29.
- Burnham, K.P., 2004. Multimodel inference: understanding AIC and BIC in model selection. *Sociological Methods & Research* 33, 261–304.
- Burnham, K.P., Anderson, D.R., 2002. *Model Selection and Multi-Model Inference: A Practical Information-Theoretic Approach*, second ed. Springer-Verlag, New York.
- Cermeno, P., Dutkiewicz, S., Harris, R.P., Follows, M., Schofield, O., Falkowski, P., 2008. The role of nutricline depth in regulating the ocean carbon cycle. *Proceedings of the National Academy of Sciences of the United States of America* 105, 20344–20349.
- Chassot, E., Bonhommeau, S., Dulvy, N.K., Mélin, F., Watson, R., Gascuel, D., Le Pape, O., 2010. Global marine primary production constrains fisheries catches. *Ecology Letters* 13, 495–505.
- Chavez, F.P., Ryan, J., Lluch-Cota, S.E.S., Niquen, C.M., 2003. From anchovies to sardines and back: multidecadal change in the Pacific Ocean. *Science* 299, 217–221.
- Chavez, F.P., Messie, M., Pennington, J.T., 2011. Marine primary production in relation to climate variability and change. *Annual Review of Marine Science* 3, 227–260.
- Cox, P.M., Betts, R.A., Jones, C.D., Spall, S.A., Totterdell, I.J., 2000. Acceleration of global warming due to carbon-cycle feedbacks in a coupled climate model. *Nature* 408, 184–187.
- Evans, E.H., Gordon, H.R., 1994. Coastal zone color scanner “system calibration”: A retrospective examination. *Journal of Geophysical Research* 99, 7293–7307.
- Falkowski, P., Wilson, C., 1992. Phytoplankton productivity in the North Pacific ocean since 1900 and implications for absorption of anthropogenic CO₂. *Nature* 358, 741–743.
- Field, C.B., Behrenfeld, M.J., Randerson, J.T., 1998. Primary production of the biosphere: integrating terrestrial and oceanic components. *Science* 281, 237–240.
- Geider, R.J., 1987. Light and temperature-dependence of the carbon to chlorophyll-a ratio in microalgae and cyanobacteria – implications for physiology and growth of phytoplankton. *New Phytologist* 106, 1–34.
- Goes, J.L., Thoppil, P.G., Gomes, H.R., 2005. Warming of the Eurasian landmass is making the Arabian sea more productive. *Science* 308, 545–548.
- Gregg, W.W., Conkright, M.E., 2002. Decadal changes in global ocean chlorophyll. *Geophysical Research Letters* 29, 1730–1734.
- Gregg, W.W., Conkright, M.E., Ginoux, P., O’Reilly, J.E., Casey, N.W., 2003. Ocean primary production and climate: global decadal changes. *Geophysical Research Letters* 30, 1813–1909.
- Gregg, W.W., Casey, N.W., McClain, C.R., 2005. Recent trends in global ocean chlorophyll. *Geophysical Research Letters* 32, 1–5.
- Hamme, R.C., Webley, P.W., Crawford, W.R., Whitney, F.A., DeGrandpre, M.D., Emerson, S.R., Eriksen, C.C., Giesbrecht, K.E., Gower, J.F.R., Kavanaugh, M.T., Pena, M.A., Sabine, C.L., Batten, S.D., Coogan, L.A., Grundle, D.S., Lockwood, D., 2010. Volcanic ash fuels anomalous plankton bloom in subarctic northeast Pacific. *Geophysical Research Letters* 37, 1–5.
- Hastie, T., Tibshirani, R., 1986. Generalized additive models. *Statistical Science* 1, 297–318.
- Henson, S.A., Sarmiento, J.L., Dunne, J.P., Bopp, L., Lima, I., Doney, S.C., John, J., Beaulieu, C., 2010. Detection of anthropogenic climate change in satellite records of ocean chlorophyll and productivity. *Biogeosciences* 7, 621–640.
- Hofmann, M., Worm, B., Rahmstorf, S., Schellnhuber, H.J., 2011. Declining ocean chlorophyll under unabated anthropogenic CO₂ emissions. *Environmental Research Letters* 6.
- Huot, Y., Babin, M., Bruyant, F., Grob, C., Twardowski, M.S., Claustre, H., 2007. Does chlorophyll a provide the best index of phytoplankton biomass for primary productivity studies? *Biogeosciences Discussion* 4, 707–745.
- Irwin, A.J., Finkel, Z.V., 2009. Mining a sea of data: deducing the environmental controls of ocean chlorophyll. *PLoS One* 3, 1–6.
- Jickells, T.D., 1998. Nutrient biogeochemistry of the coastal zone. *Science* 281, 217–222.
- Kim, Y.J., Gu, C., 2004. Smoothing spline Gaussian regression: more stable computation via efficient approximation. *Journal of the Royal Statistical Society: Series B* 66, 337–356.
- Legendre, P., Legendre, L., 1998. *Numerical Ecology*, second ed. Elsevier Science, Amsterdam.
- Litzow, M.A., Ciannelli, L., 2007. Oscillating trophic control induces community reorganization in a marine ecosystem. *Ecology Letters* 10, 1124–1134.
- Mackas, D.L., 2011. Does blending of chlorophyll data bias temporal trend? *Nature: Brief communications arising* 472, E4–E5.
- Martinez, E., Antoine, E., Ortenzio, F., Gentili, B., 2009. Climate-driven decadal-scale oscillations of Oceanic Phytoplankton. *Science* 326, 1253–1256.
- McClain, C.R., Signorini, S.R., 2004. Subtropical gyre variability observed by ocean-color satellites. *Deep Sea Research Part II* 51, 281–301.
- McQuatters-Gollop, A., Reid, P.C., Edwards, M.E., Burkhill, P.H., Castellani, C., Batten, S., Gieskes, W., Beare, D., Bidigare, R.R., Head, E., Johnson, R., Kahru, M., Koslow, A.J., Angelica, P., 2011. Is there a decline in marine phytoplankton? *Nature: Brief communications arising* 472, E6–E7.
- Montes-Hugo, M., Doney, S.C., Ducklow, H.W., Fraser, W., Martinson, D., Stammerjohn, S.E., Schofield, O., 2009. Recent changes in phytoplankton communities associated with rapid regional climate change along the western Antarctic Peninsula. *Science* 323, 1470–1473.
- Murtugudde, R., Beauchamp, R.J., McClain, C.R., Lewis, M.R., Busalacchi, A., 2002. Effects of penetrative radiation on the upper tropical ocean circulation. *Journal of Climate* 15, 470–486.
- Nixon, S.W., 1995. Coastal marine eutrophication: a definition, social causes and future concerns. *Ophelia* 41, 199–219.
- O’Connor, M.I., Piehler, M.F., Leech, D.M., Anton, A., Bruno, J.F., 2009. Warming and resource availability shift food web structure and metabolism. *PLoS Biology* 7.
- Olonschek, D., Hofmann, M., Worm, B., Schellnhuber, H.J., 2013. Decomposing the effects of ocean warming on chlorophyll a concentrations into physically and biologically driven contributions. *Environmental Research Letters* 8, 014043.
- O’Reilly, J.E., Maritorena, S., Siegel, D., O’Brien, M.C., Toole, D., Mitchell, B.G., Kahru, M., Chavez, F.P., Strutton, P., Cota, G., Hooker, S.B., McClain, C.R., Carder, K.L., Muller-Karger, F., Harding, L., Magnuson, A., Phinney, D., Moore, G.F., Aiken, J., Arrigo, K.R., Letelier, R., Culver, M., 2000. *Ocean Color Chlorophyll a Algorithms for SeaWiFS, OC2, and OC4: Version 4, SeaWiFS Postlaunch Technical Report Series, vol. 11*. NASA, Goddard Space Flight Center, Greenbelt, Maryland.
- Peierls, B., Caraco, N., Pace, M., Cole, J., 1991. River nitrogen export linked to human population density. *Nature* 350, 386–387.
- Polovina, J.J., Woodworth, P.A., 2012. Declines in phytoplankton cell size in the subtropical oceans estimated from satellite remotely-sensed temperature and chlorophyll, 1998–2007. *Deep Sea Res. Part II* 77–80, 82–88.
- Polovina, J.J., Howell, E.A., Abecassis, M., 2008. Ocean’s least productive waters are expanding. *Geophysical Research Letters* 35, L03618.
- Raitsos, D.E., Reid, P.C., Lavender, S.J., Edwards, M., Richardson, A.J., 2005. Extending the SeaWiFS chlorophyll data set back 50 years in the northeast Atlantic. *Geophysical Research Letters* 32, 1–4.
- Redfield, A.C., 1958. The biological control of chemical factors in the environment. *American Scientist* 46, 205–221.
- Reid, P.C., 1975. Large-scale changes in North Sea phytoplankton. *Nature* 257, 217–219.
- Reid, P.C., Edwards, M., Hunt, H.G., Warner, A.J., 1998. Phytoplankton change in the North Atlantic. *Nature* 391, 546.
- Richardson, A.J., Schoeman, D.S., 2004. Climate impact on plankton ecosystems in the Northeast Atlantic. *Science* 305, 1609–1612.
- Rydzewski, R., Dunne, J.P., 2011. A measured look at ocean chlorophyll trends. *Nature: Brief communications arising* 472, E5–E6.
- Ryther, J.H., 1969. Photosynthesis and fish production in the sea. *Science* 166, 72–76.
- Saba, V.S., Marjorie, A., Friedrichs, A., Carr, M.-E.M.E., Antoine, D., Armstrong, R.A., Asanuma, R., Aumont, O., Bates, N.N.R., Behrenfeld, M.J.M.J., Benington, V., Bopp, L., Bruggeman, J., Buitenhuis, E.E.T., Church, M.J.M.J., Ciotti, A.M.A.M., Doney, S.C., Dowell, M., Dunne, V., Friedrichs, M.A.M., Asanuma, I., Dunne, J., Dutkiewicz, S., Gregg, W., Hoepffner, N., Hyde, K.J.W., Ishizaka, J., Kameda, T., Karl, D.M., Lima, I., Lomas, M.W., Marra, J., McKinley, G.A., Melin, F., Moore, J.K., Morel, A., O’Reilly, J., Salihoglu, B., Scardi, M., Smyth, T.J., Tang, S.L., Tjiputra, J., Uitz, J., Vichi, M., Waters, K., Westberry, T.K., Yool, A., Mélin, F., 2010. Challenges of modeling depth-integrated marine primary productivity over multiple decades: A case study at BATS and HOT. *Global Biogeochemical Cycles* 24, 1–21.
- Saulquin, B., Fablet, R., Mangin, A., Mercier, G., Antoine, D., D’Andon, F., 2013. Detection of linear trends in multi-sensor time series in presence of auto-correlated noise: application to the chlorophyll-a SeaWiFS and MERIS datasets and extrapolation to the incoming Sentinel 3 - OLCI mission. *Journal of Geophysical Research-Oceans* 118, 3752–3763.
- Schwarz, G., 1978. Estimating the dimension of a model. *Annals of Statistics* 6, 461–464.
- Sokal, R.R., Rohlf, F.J., 1995. *Biometry – The Principles and Practice of Statistics in Biological Research*, third ed. W.H. Freeman, New York.
- Steinacher, M., Joos, F., Frolicher, T.L., Bopp, L., Cadule, P., Cocco, V., Doney, S.C., Gehlen, M., Lindsay, K., Moore, J.K., Schneider, B., Segsneider, J., 2010. Projected 21st century decrease in marine productivity: a multi-model analysis. *Biogeosciences* 7, 979–1005.
- Taucher, J., Oschlies, A., 2011. Can we predict the direction of marine primary production change under global warming? *Geophysical Research Letters* 38.
- Vantrepotte, V., Melin, F., 2009. Temporal variability of 10-year global SeaWiFS time-series of phytoplankton chlorophyll a concentration. *ICES Journal of Marine Science* 66, 1547–1556.
- Venrick, E.L., McGowan, J.A., Cayan, D.R., Hayward, T.L., 1987. Climate and chlorophyll a: long-term trends in the Central North Pacific Ocean. *Science* 238, 70–72.
- Walsh, W.A., Kleiber, P., 2001. Generalized additive model and regression tree analyses of blue shark (*Prionace glauca*) catch rates by the Hawaii-based commercial longline fishery. *Fisheries Research* 53, 115–131.
- Ware, D.M., Thomson, R.E., 2005. Bottom-up ecosystem trophic dynamics determine fish production in the Northeast Pacific. *Science* 308, 1280–1284.
- Wernand, M.R., van der Woerd, H.J., 2010. Spectral analysis of the Forel-Ule ocean colour comparator scale. *Journal of the European Optical Society: Rapid Publications* 5, 10014s.
- Wilson, E., 1927. Probable inference, the law of succession, and statistical inference. *Journal of American Statistical Association* 22, 209–212.
- Wood, S.N., 2003. Thin plate regression splines. *Journal of the Royal Statistical Society: Series B (Statistical Methodology)* 65, 95–114.
- Wood, S.N., 2004. Stable and efficient multiple smoothing parameter estimation for generalized additive models. *Journal of American Statistical Association* 99, 673–686.
- Wood, S., 2006. *Generalized Additive Models: An Introduction with R*. Biometrics, Chapman & Hall/CRC, Boca Raton, FL.